Energy & Environmental Science

PAPER

View Article Online
View Journal | View Issue

Cite this: *Energy Environ. Sci.*, 2016, **9**, 2603

The critical role of lithium nitrate in the gas evolution of lithium–sulfur batteries†

Anna Jozwiuk,*[a] Balázs B. Berkes,*[a] Thomas Weiß,[b] Heino Sommer,[ab] Jürgen Janek[ac] and Torsten Brezesinski*[a]

Received 15th March 2016,
Accepted 13th June 2016

DOI: 10.1039/c6ee00789a

www.rsc.org/ees

Sulfur–carbon composites are promising next generation cathode materials for high energy density lithium batteries and thus, their discharge and charge properties have been studied with increasing intensity in recent years. While the sulfur-based redox reactions are reasonably well understood, the knowledge of deleterious side reactions in lithium–sulfur batteries is still limited. In particular, the gassing behavior has not yet been investigated, although it is known that lithium metal readily reacts with the commonly used ethereal electrolytes. Herein, we describe, for the first time, gas evolution in operating lithium–sulfur cells with a diglyme-based electrolyte and evaluate the effect of the polysulfide shuttle-suppressing additive $LiNO_3$. The use of the combination of two operando techniques (pressure measurements and online continuous flow differential electrochemical mass spectrometry coupled with infrared spectroscopy) demonstrates that the additive dramatically reduces, but does not completely eliminate gassing. The major increase in pressure occurs during charge, immediately after fresh lithium is deposited, but there are differences in gas generation during cycling depending on the addition of $LiNO_3$. Cells with $LiNO_3$ show evolution of N_2 and N_2O in addition to CH_4 and H_2, the latter being the main volatile decomposition products. Collectively, these results provide novel insight into the important function of $LiNO_3$ as a stabilizing additive in lithium–sulfur batteries.

Broader context

The lithium–sulfur system is without doubt one of the most promising next generation battery technologies. However, there are still many open questions and issues related to both its stability and safety that need to be addressed before full commercialization of lithium–sulfur batteries can be achieved. Major issues are fast capacity degradation and gas generation due to the polysulfide shuttle and decomposition of electrolyte components, respectively, the latter being strongly related to the lithium metal anode. Lithium nitrate is typically used as a stabilizing additive, but its function in operating lithium–sulfur batteries is largely unknown. Here, we present data on the gassing behavior of practical lithium–sulfur cells from in operando pressure measurements as well as online continuous flow differential electrochemical mass spectrometry/infrared spectroscopy. The results help to better understand failure mechanisms and thus to develop new electrolyte components and additives to improve the safety and performance of lithium–sulfur batteries.

1 Introduction

The lithium–sulfur (Li–S) system forms the chemical basis for one of the most promising next generation battery technologies with a high theoretical energy density of 2500 W h kg^{-1} (or 2800 W h L^{-1}) and with sulfur as a cheap and abundant cathode material.[1] It relies on the stepwise reaction of S_8 through intermediate lithium polysulfides of different chain lengths (Li_2S_x with $2 \leq x \leq 8$) to Li_2S during discharge and back to elemental sulfur during charge.[2] Simultaneously, lithium is dissolved and re-deposited at the anode, respectively. In the past decade, research has been conducted mainly to improve the cathode design, *e.g.*, by the synthesis of novel carbons and composite structures, with the goal to better trap the lithium polysulfide species and improve their interactions with the host material.[3–8] This leads to higher sulfur utilization and therefore, higher specific capacities and longer battery life. In addition, investigations have been performed to further understand reaction and conversion mechanisms of lithium polysulfides during cycling through advanced *in situ* and operando techniques.[2,9] Major challenges of Li–S batteries

[a] *Battery and Electrochemistry Laboratory, Institute of Nanotechnology, Karlsruhe Institute of Technology, Hermann-von-Helmholtz-Platz 1, 76344 Eggenstein-Leopoldshafen, Germany. E-mail: anna.jozwiuk@kit.edu, balazs.berkes@kit.edu, torsten.brezesinski@kit.edu*
[b] *BASF SE, 67056 Ludwigshafen, Germany*
[c] *Institute of Physical Chemistry, Justus-Liebig-University Gießen, Heinrich-Buff-Ring 17, 35392 Gießen, Germany*
† Electronic supplementary information (ESI) available. See DOI: 10.1039/c6ee00789a

still are fast capacity fading caused by the polysulfide shuttle and decomposition of the ethereal electrolyte solvent(s),[10–12] which are mainly related to the lithium metal anode. The most commonly used solvents are 1,3-dioxolane (DOL) and 1,2-dimethoxyethane (DME) as a mixture or longer chain glymes.[13] The shuttle reaction, briefly, is a typical problem of conversion-type batteries where oxidized/reduced species diffuse to the opposite electrode site and are re-oxidized/re-reduced. Lithium nitrate ($LiNO_3$) was found to be the most effective shuttle suppressor when used as an additive. Its degradation products form a protective passivation layer on lithium which results in higher Coulombic efficiencies.[14,15] Unfortunately, $LiNO_3$ is continuously consumed during cycling.[16] Typically, the problems related to the anode are compensated by use of excess electrolyte. This, however, decreases the gravimetric energy density considerably. The majority of publications also report low sulfur loadings resulting in improved cycling performance by not stressing the anode as much. To reach energy densities comparable to or higher than the state of the art lithium-ion batteries, high sulfur loadings (≥ 5 mg cm^{-2}) and low amounts of electrolyte (electrolyte/sulfur ratio $\leq 4:1$ by weight) are needed.[17,18] However, under such conditions, Li–S batteries usually fail below a hundred cycles because of severe anode corrosion.[19]

In recent years, a few *ex situ* studies have been performed to gain a better understanding of failure mechanisms with respect to decomposition reactions at the anode. For example, Aurbach and coworkers investigated the decomposition products on lithium in the presence of DOL/LiTFSI/$LiNO_3$ through Fourier transform infrared (FTIR) spectroscopy and X-ray photoelectron spectroscopy (XPS) and found poly-DOL-oligomers as well as Li_xNO_y and Li_xSO_y on the surface.[14] The generation of the latter inorganic products was confirmed by a different study using XPS.[20] This study also revealed that only in the presence of both lithium polysulfides and $LiNO_3$ a relatively stable and compact solid-electrolyte interphase (SEI) on lithium is formed. Overall, the *ex situ* examination of reactive electrode surfaces is a major challenge (*e.g.*, with respect to contamination from the atmosphere before and during analysis) and thus, interpretation of data should be carried out with care. To the best of our knowledge, no *in situ* study on electrolyte decomposition reactions in Li–S batteries has been reported in the literature so far. Particularly, monitoring of gas formation should provide a better insight into degradation processes. Only if decomposition products are clearly identified can a better understanding of failure mechanisms in Li–S cells be gained and with that, novel additives suggested or better electrolyte components developed to protect the lithium metal anode.

Herein, we investigate, for the first time, the gassing processes in operating Li–S cells using diglyme/LiTFSI electrolyte (with and without $LiNO_3$) by means of pressure measurements as well as simultaneous online analysis of the gases by mass spectrometry (MS) and FTIR spectroscopy. For the gas analysis, we have designed a special battery cell, in which a typical anode/separator/cathode setup is implemented and have established a novel and unique flow-through differential electrochemical mass spectrometry (DEMS) system.[21] Our approach to add a gas FTIR cell to this system—referred to as differential electrochemical infrared spectroscopy (DEIRS) in the following—helped to facilitate the identification of gas molecules.[22] First, we show the gassing of Li–S cells with and without $LiNO_3$ in general. Then, we focus on the nature of the gaseous products and on their generation patterns during cycling and open circuit voltage (OCV) periods. Isotopically labeled nitrate was used to correctly identify the evolution of N_2 and N_2O.

2 Results and discussion

To obtain full information on the gassing behavior of conventional Li–S batteries, we have used the combination of in operando DEMS-DEIRS and pressure measurements. The electrolyte solvent was chosen to be diglyme instead of the more commonly used mixture of DOL and DME. The shorter chain ethers are too volatile to be used in a flow through DEMS-DEIRS setup, like that established in our laboratory (diglyme has only 1/16th or 1/23rd of the vapor pressure of DME or DOL, respectively).[21,22] However, various glymes have been used before and they give similar voltage profiles during charge and discharge.[13]

2.1 Pressure measurements

To investigate how much gas is formed during cycling, pressure measurements were performed first. Fig. 1 shows the pressure trends with respect to the individual cycling profile in diglyme using LiTFSI as the sole supporting salt and additionally containing $LiNO_3$ as an additive.

After assembling, each system was allowed to equilibrate for 48 h prior to cycling to guarantee a stable pressure background (only the last 8 h of the OCV period are shown for clarity in Fig. 1a and b). ΔP was calculated from the absolute pressure according to: $\Delta P(t) = P(t) - P(40\text{ h})$. This means the pressure after 40 h was subtracted from the measured values of P. Thus, for the sake of clarity, ΔP represents a relative value. Both cells show about the same pressure trend in the formation (first) cycle at C/10, with a small increase at the beginning of discharge as well as during the entire charge by about 2 mbar. Major differences can be seen upon further cycling at C/5. For the cell with $LiNO_3$ (Fig. 1a), pressure always increases during charging (lithium deposition on the anode) by <1 mbar, while a decrease (>1 mbar) can be observed on discharge (see also Fig. S1, ESI† with a smaller ΔP range for more details). This results in an overall slight decrease of a few mbar after multiple cycles. A possible explanation for that could be that gases are produced spontaneously as soon as the electrolyte comes into contact with the fresh lithium anode, *i.e.*, before the pressure sensor is connected to the cell. A decrease thereafter can only be explained by either dissolution of the gases within the electrolyte or consumption of certain gaseous products by reactions to form *e.g.*, solid components or by the volume change of the electrodes. Another possibility is that sulfur from the cathode is being dissolved in the form of anionic species. This induces the dissolution of the lithium anode, causing a decrease in its volume and with that a decrease of the total pressure in the cell. The effect of volume change of the lithium anode on the pressure change in the system is shown in Fig. S2 (ESI†). In contrast, the

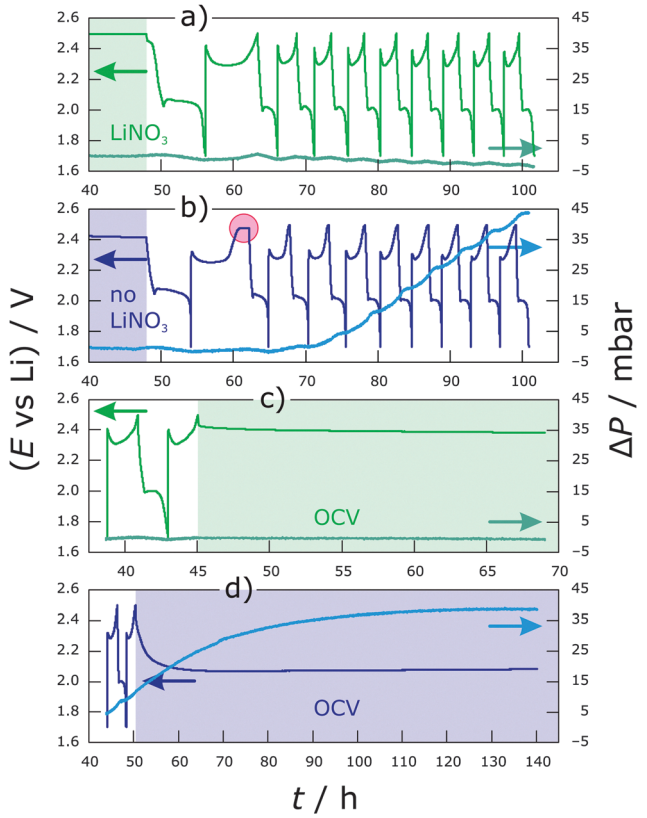

Fig. 1 Pressure trends with dependence on the charge/discharge profile for Li–S cells using the diglyme/LiTFSI electrolyte with (a and c) and without $LiNO_3$ (b and d). The red circle indicates an infinite charge region due to the polysulfide shuttle (charging is terminated by a time limit) and shaded areas represent OCV periods before and after cycling.

slope of the pressure–time curve is always positive for the cell without $LiNO_3$ from the 4th cycle onwards (Fig. 1b). The pressure increases significantly by 2–4 mbar (increasing with the cycle number) during a single charge step, and there is further pressure increase until the middle of discharge. Overall, an increase of >40 mbar is observed after 8 cycles—from the 4th cycle onwards it increases linearly with a rate of 1.5 mbar h^{-1}. Applying the ideal gas law, an increase in pressure by 10 mbar in our cell (dead volume of ~6 mL) corresponds to an amount of about 2.5×10^{-3} mmol or a gas volume of about 55 μL. Assuming a 1-electron process for gas evolution, this means a charge of 67 μA h. Fig. 1c and d show the pressure trend with respect to the voltage change during OCV after cycling. The pressure does not change significantly in the cell with $LiNO_3$ and a stable voltage of 2.4 V is reached within less than 1 h (Fig. 1c and Fig. S1, ESI†). This suggests that a relatively stable SEI has been formed on lithium, thereby preventing shuttling or other decomposition reactions. On the other hand, when no $LiNO_3$ is added, a further increase in pressure by ~30 mbar is observed for >70 h, while the cell potential drops over time to 2.1 V (Fig. 1d). This indicates ongoing decomposition reactions.

2.2 DEMS-DEIRS measurements

To identify the gases formed during cycling, DEMS-DEIRS was conducted on nitrate-containing and nitrate-free Li–S batteries. Fig. 2 shows the ion currents for m/z = 2, 15 and 16 with respect to the voltage profile measured in cells with $LiNO_3$. The m/z = 2 channel corresponds to H_2 (beneath the H_2 fragmented from the volatile diglyme in the MS). It is generated already in the initial OCV period (7 h for the DEMS-DEIRS experiments) due to the reaction of the electrolyte with lithium, later at the very beginning of the first discharge and during each subsequent charge cycle. It seems that less H_2 is produced as the cell is cycled. During charge, a fresh lithium surface is created which could cause the reductive formation of H_2 before the formation of the SEI layer. Another gaseous compound we were able to identify during cycling, though in small quantity, is CH_4. The signals for m/z = 15 and 16 indicate its existence, and the characteristic FTIR vibrations (Fig. 4, inset) unequivocally identify it. Both the MS and FTIR data show very similar behavior. The dramatic change of the MS signals during the first OCV period and in the first cycle is caused by electrolyte signal fluctuation (m/z = 45 and 59, also fragments of diglyme, follow the very same trend) and the presence of O_2 that is gradually purged out.

There is virtually no generation of CH_4 until the second cycle and this is further supported by FTIR, making the simultaneous use of vibrational spectroscopy even more powerful. CH_4 evolves in an alternating fashion to H_2 in each discharge, but not from the beginning (strong increase from the voltage dip between the discharge plateaus), and increases with the cycle number. The voltage dip indicates supersaturation of S^{2-} and an increased electrolyte resistance.[23,24] It is likely that the reactive Li is protected by an SEI layer formed through reactions with $LiNO_3$ since the cell without $LiNO_3$ shows more pronounced gassing. Therefore, the reductive decomposition of the electrolyte solvent (diglyme) occurs at the cathode side. The cathode still shows a quite negative potential even in a fully charged state with reference to the standard hydrogen electrode (*ca.* −500 mV). However, the most intense CH_4 evolution can be observed with decreasing cathode potential, also supporting this assumption. At the beginning, the electrocatalytically active carbon surface

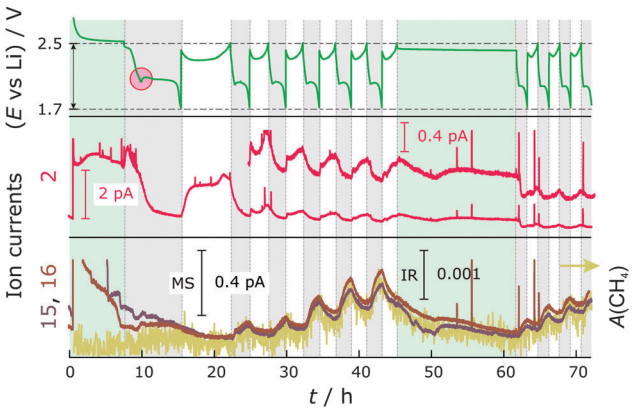

Fig. 2 Top: Voltage profile of a Li–S cell with $LiNO_3$. Middle: MS ion current for m/z = 2. Bottom: MS ion current for m/z = 15 and 16 as well as the integrated FTIR signal ($A(CH_4)$) of the Q-branch of CH_4 (yellow) at 3015 cm^{-1}. The red circle indicates a voltage dip between the discharge plateaus. Green shaded areas represent OCV periods, while discharge and charge regions are highlighted in grey and white, respectively.

is blocked by the impregnated sulfur that gradually dissolves during cycling, making reactive surfaces available. The generation of H_2 could be either due to remaining traces of H_2O in the cell components/electrolyte or a decomposition product of diglyme. However, H_2O contamination presumably contributes only initially to the H_2 evolution. We hypothesize that in addition to the formation of CH_4 an alcohol (*e.g.*, methanol or longer chain alcohol) is formed in the reduction process of diglyme during discharge. This "reaction product" can be reduced to form H_2 in the next charge cycle. We note that the SEI might not only be Li^+ conducting, but also H^+ conducting. CH_4 is most likely generated from the methyl group of diglyme. Similarly, CH_4 should be generated from DME in DOL/DME-based electrolytes. To test whether the SEI on lithium really prevents further decomposition reactions, an OCV period of 16 h was added after cycling. As in the pressure measurements, the cell potential stabilized quickly at 2.4 V and the signals for H_2 and CH_4 decreased. Thereafter, the battery was cycled for a few more hours and the trends for CH_4 and H_2 gas evolution are very similar to the previous cycles.

We also observe some trends for ions with m/z = 28 and 44 with Li–S cells containing $LiNO_3$ during cycling. The corresponding gases could be N_2 or CO (m/z = 28) and N_2O or CO_2 (m/z = 44). To reveal the identity and origin of the gases concealed by these masses, experiments with isotopically labeled nitrate ($Li^{15}NO_3$ and $Li^{15}N^{18}O_3$) were conducted (Fig. 3). The use of labeled nitrate identified the gases as N_2 (m/z = 28 for N_2 or 30 for $^{15}N_2$) and N_2O (m/z = 44 for N_2O, 46 for $^{15}N_2O$ or 48 for $^{15}N_2{}^{18}O$) and at the same time proves their origin from the added $LiNO_3$ and not from contamination, *e.g.*, air leaks or H_2O in the electrolyte. These results should help to further understand the role and mechanism of the polysulfide shuttle-suppressing additive in Li–S batteries. During each charge, especially increasing towards the end of the charge cycle, N_2 and N_2O are generated, meaning that the nitrogen from nitrate is reduced. Their formation overlaps exactly with that of H_2 gas during cycling. A feasible side product could be Li_2O, which deposits on lithium and is a part of the forming SEI. It is possible that N_2 and N_2O further react with lithium to create Li_3N and Li_xNO_y species.[14,20] This could explain why the pressure decreases during discharge in the nitrate-containing system.

In the experiments without $LiNO_3$, the generation of H_2 and CH_4 is much more pronounced (higher signal to noise ratio of the signals). Fig. 4 shows the trend of the MS and FTIR signals. Similar to the Li–S cells with $LiNO_3$, in the first cycle, H_2 is produced at the beginning of discharge and during the entire charge. In subsequent cycles, H_2 is evolved further and the amount seems to gradually exceed that which can effectively be purged out. There is a much steeper increase of H_2 generation towards the end of charge than in cells containing additives. This might be because there is no protective layer on the freshly deposited lithium, unlike in the case with additive. Also different is the appearance of a H_2 peak at the voltage dip of discharge. CH_4 is again produced mainly during discharge, but in higher amounts. As is evident, its evolution contributes significantly to the pressure increase shown in Fig. 1. We also observe further

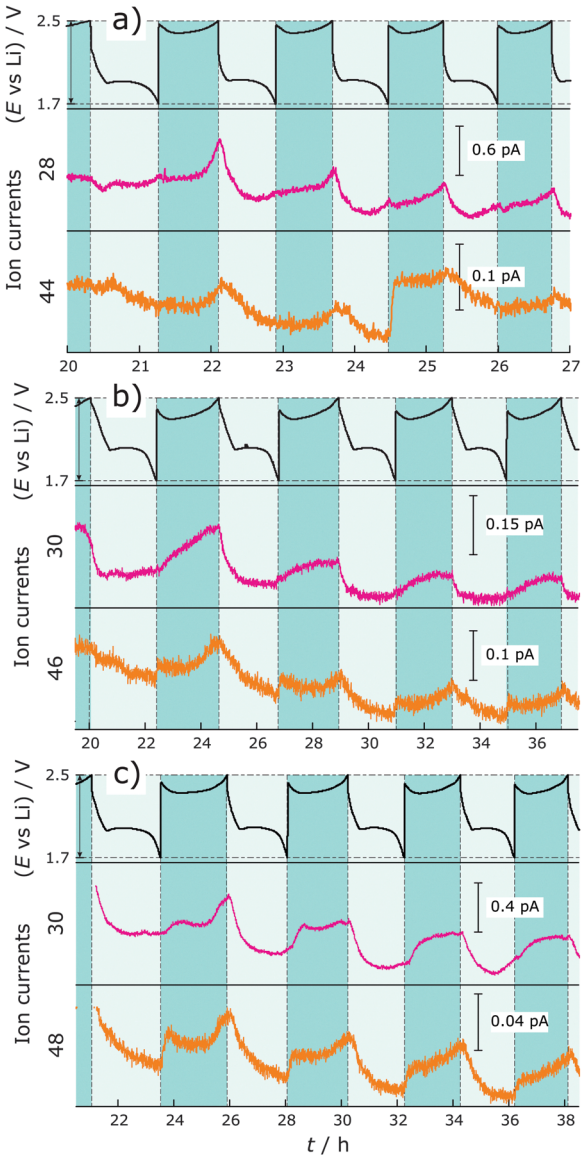

Fig. 3 DEMS measurements on Li–S cells with additive: $LiNO_3$ (a), $Li^{15}NO_3$ (b) and $Li^{15}N^{18}O_3$ (c). Top: Voltage profile. Middle: MS ion current for N_2 or $^{15}N_2$ with m/z = 28 or 30, respectively. Bottom: MS ion current for N_2O, $^{15}N_2O$ or $^{15}N_2{}^{18}O$ with m/z = 44, 46 or 48, respectively. Discharge and charge regions are highlighted in grey and cyan, respectively.

increased CH_4 production during the OCV period after cycling, which is consistent with the pressure trend for the cells without $LiNO_3$. Without $LiNO_3$ the SEI formed on Li (if at all) is less stable. Most probably, Li reacts instantaneously with the electrolyte when assembling the cell. During electrochemical cycling, Li becomes more "reactive" due to continuous dissolution/deposition which increases the surface area. Without the protective SEI layer, diglyme readily reacts with Li, which is probably more reactive when charging the battery (Li deposition on the anode)—with that the signal of CH_4 increases in the charge cycle. As evident from the pressure measurements and MS/IR data, the reduction of diglyme continues in the OCV period (increasing pressure and methane signal). Therefore, it must be a chemical process occurring on lithium. Eqn (1)–(3) below describe possible reactions of $LiNO_3$ in

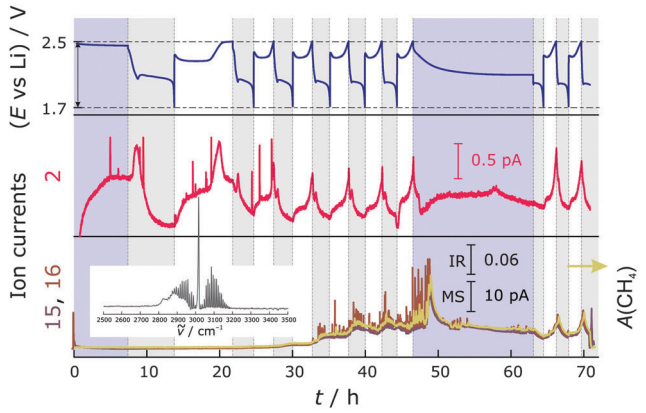

Fig. 4 Top: Voltage profile of a Li–S cell without $LiNO_3$. Middle: MS ion current for m/z = 2. Bottom: MS ion current for m/z = 15 and 16 as well as the integrated FTIR signal ($A(CH_4)$) of the Q-branch of CH_4 (yellow) at 3015 cm^{-1}. Inset: FTIR spectrum of CH_4 measured with the DEIRS setup at maximum concentration. Purple shaded areas represent OCV periods, while discharge and charge regions are highlighted in grey and white, respectively.

the system—which are likely to be spontaneous according to thermodynamic calculations—and Scheme 1 summarizes the gassing behavior in cells with and without additive.

$$LiNO_3 + 2Li \rightarrow Li_2O + LiNO_2 \quad \Delta_rG = -472.56 \text{ kJ mol}^{-1} \quad (1)$$

$$8LiNO_2 + S_8 \rightarrow 4Li_2S_2O_3 + 4N_2O \quad (2)$$

$$N_2O + 2Li \rightarrow N_2 + Li_2O \quad \Delta_rG = -664.90 \text{ kJ mol}^{-1} \quad (3)$$

According to eqn (2), sulfur reacts with $LiNO_2$. Given that sulfur is formed in the charge cycle, the formation of N_2O, which reacts further with Li to give N_2 (eqn (3)), is expected to occur during charge, in line with our findings. A reaction similar to that in eqn (2) has already been reported by Schmidt *et al.*[25] They studied the conversion of $NaNO_2$ to $Na_2S_2O_3$ through reaction with S_8 in a non-aqueous medium (see also gas evolution in symmetric Li–Li cells with and without the $LiNO_3$ additive in Fig. S3, ESI†). In addition, we hypothesize the formation of methyl radicals that can further react with the electrolyte to produce CH_4. However, the mechanism of this reaction might be very complex. Unveiling goes beyond the scope of the paper and further experiments are needed. Because H_2 formation is observed during the entire cycling process, it does not originate solely from water residues. It is more likely that a reaction product—*e.g.*, an alcohol—forms during discharge (*e.g.*, beneath CH_4) and further reacts to form H_2 during charge.

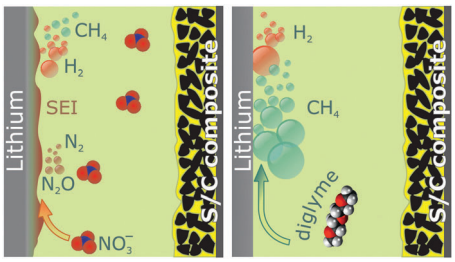

Scheme 1 Overview of the reactions producing gases in Li–S batteries with the diglyme-based electrolyte with (left) and without $LiNO_3$ (right).

Overall, the DEMS-DEIRS results are in good agreement with the pressure measurements. However, care should be taken when comparing the details. The system for pressure measurements is closed and gases can potentially further react to form other products, which may influence the pressure change. On the other hand, the flow-through cell used for DEMS-DEIRS is continuously purged and all gases, once generated, have little time for follow-up reactions.

Besides CH_4 and H_2, we were able to find other gaseous decomposition products for some experiments independent of $LiNO_3$ addition, like H_2S (m/z = 32, 33 and 34) and SO_2 (m/z = 64 and 48 and characteristic vibrations in the FTIR spectrum). However, there was no clear pattern or trend on why these gases occasionally show up. It is very likely that the generation of H_2S and SO_2 is related to the total amount of H_2O contamination in the battery cell and further experiments are needed to investigate this relationship.

3 Conclusions

This study reveals, for the first time, gas evolution in operating lithium–sulfur batteries. CH_4 and H_2 were identified as the major gaseous decomposition products, particularly during charging when a fresh lithium surface is created at the anode. We show that gassing is suppressed when $LiNO_3$ is used as an electrolyte additive. Especially, the amount of CH_4 is dramatically decreased and either very little or no H_2 is generated during discharge. Further N_2 and N_2O evolve in the charge cycles when $LiNO_3$ is present. Their generation is probably related to the formation of a relatively stable SEI on lithium and with that, suppression of the polysulfide shuttle. From our pressure measurements, it seems that these gases are consumed and possibly built into the SEI. Therefore, it would be interesting to test whether just simple addition of N_2 and/or N_2O, instead of $LiNO_3$, will give the same positive or even a better effect during cycling. Some measurements also revealed H_2S evolution independent of $LiNO_3$ addition. Its appearance could be related to the H_2O traces in the battery cell, but further work is needed to confirm this hypothesis.

4 Experimental

4.1 Materials and electrode preparation

For the preparation of the positive electrode, sulfur (Aldrich, reagent grade), Super C65 (Timcal) and Printex-XE2 (Orion) in a ratio of 1.7 : 0.5 : 0.5 were ground. Poly(vinyl alcohol) Selvol 425 (Sekisui) dissolved in a mixture of water, isopropanol and 1-methoxy-2-propanol was added to the blend and the mixture was ball-milled for 20 h to form a slurry. The slurry was then coated onto 8 μm-thick primed aluminum and dried in a vacuum at 40 °C for 16 h. The sulfur content in the electrode was 60%, with sulfur loadings of 1.7–1.8 mg cm^{-2}. Coin-type cells were assembled in an argon-filled glovebox by stacking a lithium

anode (China Lithium Ltd, size: 600 μm × 40 mm), a GF/A separator (GE Healthcare Life Sciences, Whatman, 42 mm diameter) and a cathode (40 mm diameter with a 4 mm hole in the center) using 600 μL of electrolyte. The electrolyte was either a solution of 0.325 M lithium bis(trifluoromethanesulfonyl)imide (LiTFSI, Aldrich, 99.95%) and 0.675 M lithium nitrate (Merck, 99.995%) or just 1 M lithium bis(trifluoromethanesulfonyl)imide in bis(2-methoxyethyl)ether (diglyme, Aldrich, 99.95%). The water content of all electrolytes used was <20 ppm, except that the electrolyte prepared with $Li^{15}N^{18}O_3$ had 120 ppm, as determined by Karl Fischer titration. $Li^{15}NO_3$ was prepared by addition of 1.1 eq. of Li_2CO_3 to a diluted aqueous solution of $H^{15}NO_3$ (Aldrich, 98 at% ^{15}N). Once gas evolution was completed, solid byproducts were removed from the reaction solution by filtration and the solvent was removed under reduced pressure. The remaining white solid ($Li^{15}NO_3$) was dried at 180 °C for 24 h yielding 81–96%. $Li^{15}N^{18}O_3$ was prepared from $H^{15}N^{18}O_3$ (Aldrich, 95 at% ^{18}O, 98 at% ^{15}N) according to the procedure for $Li^{15}NO_3$, yielding 61%.

4.2 Electrochemical testing

Electrochemical cycling was performed in the potential range of 1.7–2.5 V with respect to Li/Li^+ using a BioLogic VSP-300 potentiostat. The batteries were kept at rest (OCV) for several hours prior to cycling to allow for equilibration. This resulted in a similar initial potential of each cell and therefore, comparable conditions. The OCV period was set to 7 h for DEMS-DEIRS experiments and 48 h for pressure measurements (to guarantee full equilibration by temperature). Pressure measurements were performed in a temperature-controlled cabinet (ESPEC Corp. PU-1KP) set to 25 °C. After one cycle at C/10 (with 1C = 1672 mA g_{sulfur}^{-1}) was completed, the cells were cycled at charge and discharge rates of C/5. For cells without lithium nitrate, a time limit in addition to the potential limit was set to terminate the charge step and avoid shuttling.[26]

4.3 Instrumentation

Both the DEMS setup and battery design have been described elsewhere.[21,22] The same cell was used for pressure and DEMS-DEIRS measurements. A commercially available quadrupole mass spectrometer with a scan range of 1–200 Da and detection limits down to 10 ppb and a secondary electron multiplier detector was used for gas analysis (GSD 320 O2, OmniStar Gasanalysesystem, Pfeiffer Vacuum GmbH, Germany). DEIRS measurements were performed using an FTIR spectrophotometer (Bruker Tensor II) equipped with a heatable gas cell module.[22] The FTIR signal in Fig. 2 and 4 is the integrated area of the Q-branch of CH_4 at 3010–3021 cm^{-1}. For pressure measurements, one of the cell lid holes was closed with a screw, while the other one was equipped with a pressure sensor (Omega PAA33X-V-3).

Acknowledgements

We thank Sven Leuthner for preparation of the materials and electrolytes. This study is a part of the projects being funded within the BASF International Network for Batteries and Electrochemistry.

References

1 S. Evers and L. F. Nazar, *Acc. Chem. Res.*, 2013, **46**, 1135–1143.
2 M. Wild, L. O'Neill, T. Zhang, R. Purkayastha, G. Minton, M. Marinescu and G. J. Offer, *Energy Environ. Sci.*, 2015, **8**, 3477–3494.
3 X. Ji, K. T. Lee and L. F. Nazar, *Nat. Mater.*, 2009, **8**, 500–506.
4 N. Jayaprakash, J. Shen, S. S. Moganty, A. Corona and L. A. Archer, *Angew. Chem., Int. Ed.*, 2011, **50**, 5904–5908.
5 J. T. Lee, Y. Zhao, S. Thieme, H. Kim, M. Oschatz, L. Borchardt, A. Magasinski, W.-I. Cho, S. Kaskel and G. Yushin, *Adv. Mater.*, 2013, **25**, 4573–4579.
6 J. Song, T. Xu, M. L. Gordin, P. Zhu, D. Lv, Y.-B. Jiang, Y. Chen, Y. Duan and D. Wang, *Adv. Funct. Mater.*, 2014, **24**, 1243–1250.
7 A. Schneider, C. Weidmann, C. Suchomski, H. Sommer, J. Janek and T. Brezesinski, *Chem. Mater.*, 2015, **27**, 1674–1683.
8 G. Zhou, E. Paek, G. S. Hwang and A. Manthiram, *Nat. Commun.*, 2015, **6**, 7760.
9 R. Xu, J. Lu and K. Amine, *Adv. Energy Mater.*, 2015, **5**, 1500408.
10 Y. Diao, K. Xie, S. Xiong and X. Hong, *J. Power Sources*, 2013, **235**, 181–186.
11 D. Moy, A. Manivannan and S. R. Narayanan, *J. Electrochem. Soc.*, 2015, **162**, A1–A7.
12 M. Hagen, P. Fanz and J. Tübke, *J. Power Sources*, 2014, **264**, 30–34.
13 M. Barghamadi, A. S. Best, A. I. Bhatt, A. F. Hollenkamp, M. Musameh, R. J. Rees and T. Ruther, *Energy Environ. Sci.*, 2014, **7**, 3902–3920.
14 D. Aurbach, E. Pollak, R. Elazari, G. Salitra, C. S. Kelley and J. Affinito, *J. Electrochem. Soc.*, 2009, **156**, A694–A702.
15 S. S. Zhang and J. A. Read, *J. Power Sources*, 2012, **200**, 77–82.
16 A. Jozwiuk, H. Sommer, J. Janek and T. Brezesinski, *J. Power Sources*, 2015, **296**, 454–461.
17 M. Hagen, D. Hanselmann, K. Ahlbrecht, R. Maça, D. Gerber and J. Tübke, *Adv. Energy Mater.*, 2015, **5**, 1401986.
18 D. Eroglu, K. R. Zavadil and K. G. Gallagher, *J. Electrochem. Soc.*, 2015, **162**, A982–A990.
19 Y. Han, X. Duan, Y. Li, L. Huang, D. Zhu and Y. Chen, *Mater. Res. Bull.*, 2015, **68**, 160–165.
20 S. Xiong, K. Xie, Y. Diao and X. Hong, *J. Power Sources*, 2014, **246**, 840–845.
21 B. B. Berkes, A. Jozwiuk, M. Vračar, H. Sommer, T. Brezesinski and J. Janek, *Anal. Chem.*, 2015, **87**, 5878–5883.
22 B. B. Berkes, A. Jozwiuk, H. Sommer, T. Brezesinski and J. Janek, *Electrochem. Commun.*, 2015, **60**, 64–69.
23 K. Kumaresan, Y. Mikhaylik and R. E. White, *J. Electrochem. Soc.*, 2008, **155**, A576–A582.
24 T. Zhang, M. Marinescu, L. O'Neill, M. Wild and G. Offer, *Phys. Chem. Chem. Phys.*, 2015, **17**, 22581–22586.
25 M. Schmidt and R. R. Wägerle, *Angew. Chem.*, 1958, **70**, 594–595.
26 A. F. Hofmann, D. N. Fronczek and W. G. Bessler, *J. Power Sources*, 2014, **259**, 300–310.

